Research Article

Journal of Environmental Nanotechnology

Biogenic Synthesis of Silicon Dioxide Nanoparticles by *Lactiplantibacillus Plantarum*: Comparative Physicochemical and Biological Evaluation

S. Jayashree[1,2], Sadasivam Narendhran[2] and P. Saravana Kumari[1*]

[1]Department of Microbiology, Rathnavel Subramaniam (RVS) College of Arts and Science, Coimbatore, TN, India
[2]Department of Bioscience, Sri Krishna Arts and Science College, Coimbatore, TN, India
Received: 12.01.2026 Accepted: 13.02.2026 Published: 30.03.2026
*sarankumaribs@gmail.com

ABSTRACT

The increasing demand for sustainable nanotechnology has accelerated interest in biological synthesis as an eco-friendly alternative to conventional chemical routes. This study compares silicon dioxide nanoparticles (SiO_2 NPs) prepared using a *Lactiplantibacillus plantarum* mediated biogenic method with those synthesized chemically, focusing on differences in their physicochemical, structural and functional characteristics. UV–Visible spectroscopy confirmed nanoparticle formation in both samples; however, the biogenic SiO_2 exhibited a sharper absorption peak at 225 nm, attributed to microbial metabolites acting as natural capping and stabilizing agents. In contrast, the chemically synthesized nanoparticles showed a weaker peak at 220 nm, suggesting mild aggregation and lower uniformity. FTIR spectra of the biogenic nanoparticles revealed functional groups such as amides, hydroxyls and carboxylates, confirming the involvement of bacterial biomolecules in surface functionalization. XRD patterns verified the crystalline SiO_2 phase in both samples, with broader peaks indicating smaller crystallite sizes in the biogenic sample. Elemental analysis using EDAX demonstrated high purity for both nanoparticle types, with reduced carbon residues in the biogenic product. FESEM and DLS analyses showed smaller, moderately aggregated biogenic particles (194 nm) compared to larger chemically synthesized particles (332 nm). Functionally, the *L. Plantarum* derived SiO_2 NPs displayed superior antioxidant activity, achieving 75.4% DPPH inhibition, and exhibited enhanced antifungal activity against *Candida parapsilosis*, with a zone of inhibition of 27.1 ± 1.4 mm at 100 mg/mL. Overall, the findings indicate that biological synthesis provides a green, efficient and reliable strategy for producing stable, bio functional SiO_2 NPs suitable for sustainable biomedical and catalytic applications.

Keywords: Antioxidant activity; Antifungal properties; Silicon dioxide nanoparticles; Green nanotechnology.

1. INTRODUCTION

Nanotechnology has emerged as a transformative field offering novel approaches for the synthesis and application of functional materials in medicine, energy, and environmental science. Nanomaterials, defined as having at least one dimension between 1 and 100 nm, possess unique physicochemical characteristics, such as high surface-to-volume ratios and enhanced reactivity, that distinguish them from their bulk counterparts (Alcoceba *et al.* 2022; Pal *et al.* 2018). Among these, SiO_2 NPs are widely recognized for their biocompatibility, stability, and high loading capacity, making them attractive platforms in catalysis, drug delivery, and biomedicine (Cavalheiro and Teixeira, 2018; Pednekar *et al.* 2017; Vazquez *et al.* 2017). However, conventional physical and chemical routes for SiO_2 NP synthesis often require elevated temperatures, costly processing steps, and toxic reagents, raising environmental and biosafety concerns (Ding *et al.* 2023; Kumar *et al.* 2021). As a result, green synthesis approaches that employ biological components have gained increasing attention as eco-friendly and biocompatible alternatives (Albalawi *et al.* 2022).

Within this green framework, the use of microbes, particularly Lactic Acid Bacteria (LAB), has gained significant attention. The species are Generally Recognized as Safe (GRAS), belong to the RG1 biosafety category, and offer a biologically safe platform for producing biomedical materials. They act as efficient biocatalysts capable of generating several biologically reducible metal and metal-oxide nanoparticles (e.g., Ag, Au, Se, ZnO) through enzymatic reduction, proton efflux, and capping interactions with surface functional groups (Maťátková *et al.* 2022; Jamkhande *et al.* 2019; Gregirchak *et al.* 2023). However, such biological reduction mechanisms apply only to redox-active metals, and LAB cannot reduce silica precursors to form SiO_2 NPs. Instead, metabolites secreted by LAB, such as organic acids, peptides and antioxidant molecules, can functionalize the surface of SiO_2 NPs, improving biocompatibility and potentially enhancing biological activity. *Lactiplantibacillus plantarum*, a well-studied probiotic strain, has been successfully used for the synthesis of metallic nanoparticles and is noted for its intrinsic antioxidant properties, which may enhance the biological functionality of the materials produced (Mukherjee *et al.* 2022; Nyabadza *et al.* 2023).

The biomedical relevance of green-engineered nanomaterials has become increasingly important due to the global rise of antimicrobial resistance (AMR). While bacterial AMR remains a major health threat, resistant fungal infections have gained similar prominence. Among fungal pathogens, *Candida* species are leading causes of invasive infections, notably in immunocompromised individuals (Cavalheiro and Teixeira, 2018). *Candida parapsilosis* has emerged as a major agent of catheter-associated bloodstream infections. The extensive clinical use of azole antifungals, particularly fluconazole, has contributed to the emergence and spread of resistant *C. parapsilosis* strains carrying mutations such as Y132F in the *ERG11* gene (Alcoceba *et al.* 2022). Furthermore, biofilm formation by this organism significantly reduces antifungal susceptibility, complicating treatment outcomes (Martins *et al.* 2023). These interconnected scientific and clinical challenges establish a logical need for alternative, non-toxic, and effective antifungal strategies. Although microbe-mediated nanobiotechnology has largely focused on metallic nanoparticles (Ag, Au, Zn, Se) with demonstrated antifungal activity against *Candida* species (Masood *et al.* 2022; Martins *et al.* 2023), comparatively fewer studies have explored the potential of integrating probiotic-derived biomolecules with silica-based nanocarriers. This gap highlights an opportunity to investigate whether SiO_2 NPs, when functionalized through green approaches, can be tailored for enhanced therapeutic performance against resistant fungal pathogens such as Fluconazole-resistant *C. parapsilosis*. Furthermore, establishing optimized eco-friendly protocols capable of yielding SiO_2 NPs with desirable physicochemical properties while simultaneously enhancing their antifungal performance represents an important and ongoing research challenge (Mahmud and Jahangir Hossain, 2024; Ao *et al.* 2024; Ding *et al.* 2023).

Although green synthesis has been widely applied to metallic nanoparticles with documented antifungal activity, there is limited research on combining LAB-derived bioactive metabolites with SiO_2 NPs for antifungal therapy. Specifically, no studies have thoroughly investigated LAB-functionalized SiO_2 NPs as a potential strategy against Fluconazole-resistant *C. parapsilosis*. Additionally, optimized protocols for achieving stable SiO_2 NPs functionalization using microbial metabolites remain insufficiently developed. Accordingly, this study aims to functionalize SiO_2 NPs using metabolites from the probiotic strain *Lactiplantibacillus plantarum* and to characterize the resulting nanomaterials. Further, the work evaluates their antioxidant properties and antifungal efficacy against clinically relevant Fluconazole-resistant *C. parapsilosis*. This research seeks to advance sustainable nanotechnology by proposing a novel, biologically enhanced SiO_2 nanoplatform with dual antioxidant and antifungal activity to address emerging antifungal drug resistance.

2. MATERIALS AND METHODS

2.1 Materials

All chemicals used in this study were of analytical grade. Tetraethyl orthosilicate (TEOS) (≥99% (GC) Purity, Synthesis Grade, CAS No: 78-10-4), ethanol, and 2, 2-diphenyl-1-picrylhydrazyl (DPPH) were purchased from Sigma-Aldrich (USA). The fluconazole-resistant *Candida parapsilosis* strain was obtained from the Indian Institute of Microbial Technology (IMTECH), Chandigarh, India. Deionized water was used throughout the experiments.

2.1.1 DNA Extraction Method

The selected isolate was taken for DNA extraction. About 1 mL of Xploregen gDNA Extraction Buffer™ 1 was added to the beaded vial. The sample culture was then added to the beaded vial and vortexed horizontally at maximum speed for 10 minutes. Subsequently, 300 µL of Extraction Buffer™ 2 was added to the beaded vial containing the solution, and the mixture was vortexed horizontally at maximum speed for 7 minutes. The tube was centrifuged at 10,000 rpm for 3 minutes at room temperature, and 800 µL of the supernatant was transferred to a sterile 2 mL vial.

Next, 200 µL of Extraction Buffer™ 3 was added, and the contents were vortexed for 5 seconds. The mixture was centrifuged at 10,000 rpm for 2 minutes, after which 800 µL of the supernatant was transferred to a clean sterile 2 mL vial. Then, 1 mL of Extraction Buffer™ 4 was added to the supernatant and vortexed for 5 seconds. Subsequently, 700 µL of the lysate was transferred to a spin column and centrifuged at 10,000 rpm for 2 minutes. The flow-through was discarded, and the step was repeated with the remaining lysate to ensure that the entire lysate was processed through the spin column.

Following this, 600 µL of Extraction Buffer™ 5 was added to the spin column and centrifuged at 10,000 rpm for 2 minutes, and the flow-through was discarded. This was followed by the addition of 600 µL of Extraction Buffer™ 6 and centrifugation at 10,000 rpm for 2 minutes, after which the flow-through was discarded. The empty spin column was then centrifuged at 10,000 rpm for 5 minutes. The spin column was placed into a sterile 1.5 mL vial, and 30 µL of Extraction Buffer™ 7 (Elution 1) was added to the center of the column and centrifuged at 10,000 rpm for 5 minutes. Finally, the spin column was transferred to a new sterile 1.5 mL vial, discarded, and both elution tubes were stored for further processing.

2.1.2 16S rRNA Sequencing

To the PCR mixture, 2 µL of 16S Forward Primer (GGATGAGCCCGCGGCCTA), 2 µL of 16S Reverse Primer (CGGTGTGTACAAGGCCCGG), 4 µl of dNTPs (2.5 mM each), 10 µL of 10X Taq DNA Polymerase Assay Buffer, 1 µL of Taq DNA Polymerase (TAQ Master Mix – High-Fidelity DNA Polymerase, 2.5 mM dNTPs, 3.2 mM MgCl2, and PCR Enzyme Buffer; 3 U/mL), 30 µL of water, and 1 µL of DNA sample were added. DNA amplification was carried out using the thermal cycler with an initial denaturation at 94°C for 3 minutes, followed by 30 cycles consisting of denaturation at 94°C for 1 minute, annealing at 50°C for 1 minute, and extension at 72°C for 2 minutes, and a final extension at 72°C for 7 minutes.

The amplified product was sequenced using the ABI 3130 Genetic Analyzer. The sequence was compared with similar 16S rRNA sequences retrieved from the DNA database using the NCBI BLAST search. A phylogenetic tree was constructed using sequences aligned with the System Software aligner, and a distance matrix was generated using the Jukes–Cantor corrected distance model.

The *Lactiplantibacillus plantarum* strain employed for the biogenic synthesis of SiO_2 NPs was isolated from a fresh dairy curd sample collected from a local market (Tamil Nadu, India). The bacterial isolate was purified by repeated streaking on de Man–Rogosa–Sharpe (MRS) agar plates and maintained at 4°C. Molecular identification was carried out through 16S rRNA gene sequencing, and the obtained sequence was deposited in the NCBI GenBank database under the accession number PX471228. The phylogenetic relationship of the isolate with closely related *Lactiplantibacillus plantarum* species was established using MEGA X software (Fig.1).

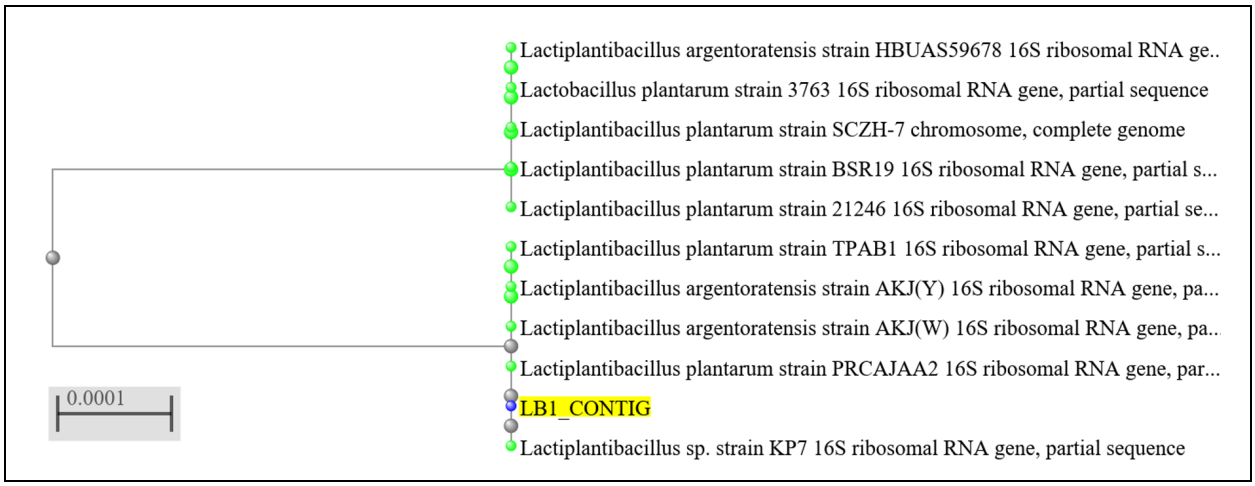


Fig. 1: Phylogenetic tree based on 16S rRNA gene sequences showing the evolutionary relationship of the *Lactobacillus* isolate used in this study (NCBI GenBank accession no. PX471228) with closely related *Lactiplantibacillus plantarum* species

2.2 Methods

2.2.1 *Lactiplantibacillus plantarum*- Mediated Synthesis of Silicon dioxide Nanoparticles (Lb–SiO_2 NPs)

The biological synthesis of SiO_2 NPs was carried out using *Lactiplantibacillus plantarum* sp. as the reducing and stabilizing agent, following a procedure adapted from Gregirchak *et al.* (2023). The bacterium was grown in LB broth at 37 °C for 48 hours under shaking (150 rpm) until a dense culture developed. The culture was centrifuged at 10,000 rpm for 10 minutes to separate the cell-free supernatant, which contained extracellular biomolecules such as proteins and polysaccharides.

For nanoparticle synthesis, 10 mL of TEOS was added dropwise to 90mL of the *Lactiplantibacillus plantarum* supernatant under continuous magnetic stirring at room temperature. The pH of the reaction mixture was adjusted to approximately 4.5 using 0.1 M ammonia solution to facilitate hydrolysis and condensation reactions. The solution was stirred for 4 hours, during which the formation of a white colloidal suspension indicated nanoparticle nucleation. The mixture was then aged at room temperature for 24 hours. The resulting precipitate was collected by centrifugation at 10,000 rpm for 15 minutes, washed repeatedly with ethanol and deionized water to remove unreacted residues, and dried at 60°C to obtain a fine white powder of *Lactiplantibacillus plantarum* -mediated SiO_2 nanoparticles (Lb– SiO_2 NPs).

For comparison, SiO_2 NPs were also synthesized via the conventional sol–gel method as described by Vazquez *et al.* (2017). In a typical procedure, 10 mL of TEOS was added dropwise to 90 mL of deionized water under constant magnetic stirring at room temperature. The pH of the solution was adjusted to 4.5 using ammonia to initiate hydrolysis of TEOS. The reaction mixture was stirred continuously for 4 hours until a white sol was formed. The sol was aged overnight at room temperature, followed by centrifugation at 10,000 rpm for 15 minutes. The precipitate was washed thoroughly with ethanol and deionized water, and the obtained SiO_2 NPs were dried at 60 °C for 6 hours. The dried powder was stored in airtight containers for further analysis.

2.2.2 Characterization of Synthesized Nanoparticles

The formation and optical properties of the nanoparticles were analyzed using UV–Visible spectroscopy (Shimadzu UV-1800) in the wavelength range 200–800 nm. Functional group analysis was carried out by Fourier Transform Infrared Spectroscopy (FTIR, PerkinElmer) in the range 4000–400cm^{-1}. The crystalline phase and structure were determined by X-ray diffraction (XRD) using a Rigaku MiniFlex 600 diffractometer with Cu-Kα radiation (λ = 1.5406 Å), operated at 40 kV and 30 mA, scanning from 10°–80° (2θ) at 2°/min. Elemental composition was evaluated by Energy-Dispersive X-ray Analysis (EDAX, Oxford Instruments) coupled with Field Emission Scanning Electron Microscopy (FESEM, Zeiss Sigma 300). FESEM micrographs were captured at different magnifications to observe morphology, and the average particle size distribution was determined using ImageJ software. Particle size and colloidal stability were further confirmed by Dynamic Light Scattering (DLS) and zeta potential analysis (Malvern Zetasizer).

2.2.3 Antioxidant Activity by DPPH Free Radical Scavenging Assay

The antioxidant potential of Lb– SiO_2 and chemically synthesized SiO_2 NPs (Ch– SiO_2) was evaluated using the 2,2-diphenyl-1-picrylhydrazyl (DPPH) assay following the method described by Mukherjee *et al.* (2022). L-ascorbic acid was used as the standard antioxidant. To ensure proper dispersion, nanoparticle suspensions were first ultrasonicated for 15 minutes using a probe sonicator and stabilized with 0.1% (w/v) Tween-80 to prevent aggregation prior to analysis. Stock suspensions of nanoparticles and standard were prepared at 120 µg/mL in distilled water and serially diluted to obtain concentrations of 20–120 µg/mL. A freshly prepared 0.1 mM DPPH solution in methanol was used as the free radical source. In each reaction, 1 mL of DPPH solution was mixed with 1 mL of sample solution and incubated in the dark for 30 minutes at room temperature. Absorbance was measured at 517 nm using a UV–Visible spectrophotometer. The scavenging activity (%) was calculated using:

$$Scavenging\ activity\ (\%) = \left(\frac{Ac-As}{Ac}\right) X\ 100 \quad \ldots (1)$$

where A_n and A_s are the absorbance of control and sample, respectively. The IC_{50} values (concentration for 50% inhibition) were determined by plotting inhibition percentage versus concentration using nonlinear regression. All tests were performed in triplicate, and results were expressed as mean ± SD.

2.2.4 Antifungal Activity Against Fluconazole-Resistant *Candida parapsilosis*

The antifungal efficacy of the synthesized nanoparticles was evaluated using the agar well diffusion method described by (Martins *et al.* 2023). *Candida parapsilosis* (fluconazole-resistant strain) was cultured on Sabouraud Dextrose Agar (SDA) and adjusted to a 0.5 McFarland standard (~1.5 × 106 CFU/mL). Stock suspensions of Lb– SiO_2 and Ch– SiO_2 nanoparticles were prepared at 10 mg/mL in sterile distilled water containing 1% (v/v) DMSO and 0.1% (w/v) Tween-80 to facilitate dispersion and prevent aggregation; the suspensions were ultrasonicated for 15 min prior to use. Serial dilutions were then performed to obtain working concentrations in the range of 20–140 µg/mL. SDA plates were uniformly inoculated with the standardized yeast suspension, and wells (6 mm diameter) were punched using a sterile borer. Each well received 50 µL of nanoparticle suspension at the desired concentration. Fluconazole (prepared in the same solvent system) served as the positive control, while the solvent mixture (distilled water + 1% DMSO + 0.1% Tween-80) without nanoparticles served as the negative control, ensuring that any observed inhibition was attributable to the nanoparticles. Plates were incubated at 37 °C for 24 h, and the diameter of the inhibition zones (mm) was measured using a digital caliper. All experiments were performed in triplicate, and data were expressed as mean ± SD. Regression analysis was used to evaluate the concentration–response relationship.

3. RESULT AND DISCUSSION

3.1 UV Visible Spectroscopic Analysis of Synthesized Nanoparticles

The optical properties of the synthesized SiO_2 NPs were analyzed using UV–Visible spectroscopy in the 200–800 nm range (Ao *et al.* 2024; Mahmud and Jahangir Hossain, 2024). The spectra for both *Lactiplantibacillus plantarum*–mediated and chemically synthesized SiO_2 NPs are shown in Fig. 2. The biogenic SiO_2 NPs exhibited a distinct and strong absorption band at 225 nm. This absorption band does not represent surface plasmon resonance (SPR), as silicon dioxide is not a plasmonic material. Instead, the peak corresponds

to intrinsic electronic transitions within Si–O_2 bonds, commonly associated with O→Si charge-transfer transitions and the presence of surface silanol groups (Si–OH), which are characteristic of nanoscale amorphous silica.

The higher absorbance intensity observed in the biogenic sample suggests improved nanoparticle dispersion and reduced aggregation, likely facilitated by biomolecules secreted by *L. Plantarum* during synthesis. These metabolites, acting as natural capping and stabilizing agents (Gregirchak *et al.* 2023), contribute to the well-defined optical features of the biogenic SiO_2 NPs. In comparison, the chemically synthesized SiO_2 NPs displayed a weaker absorption band at 220 nm, with slight reduction in peak sharpness. This lower intensity is indicative of less uniform particle formation and increased aggregation, likely due to the absence of biological stabilizers commonly present in the biogenic synthesis environment (Ao *et al.* 2024).

Overall, the UV–Vis analysis confirms successful formation of SiO_2 NPs via both green and chemical routes. However, the *L. Plantarum*–mediated synthesis resulted in better-defined electronic transition bands and more stable dispersion, highlighting the effectiveness of the biological approach for producing uniformly stabilized SiO_2 NPs.

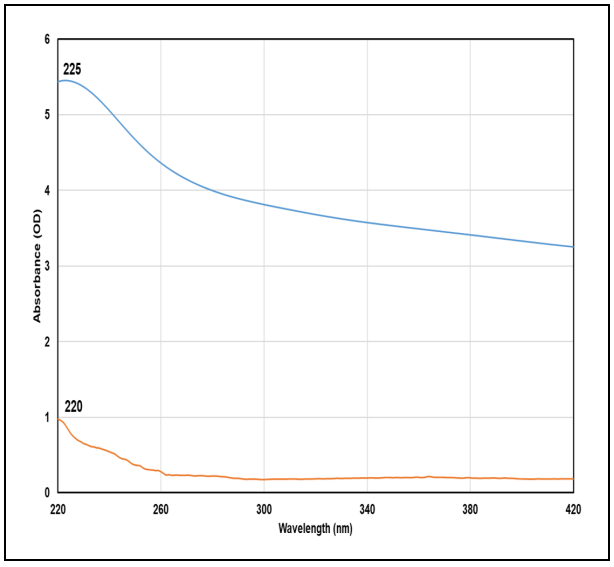


Fig. 2: UV–Visible absorption spectra of *Lactiplantibacillus* plantarum-mediated SiO_2 NPs (blue curve) and chemically synthesized SiO_2 NPs (orange curve)

3.2 FTIR Analysis of *Lactiplantibacillus plantarum sp.* Culture

Fourier Transform Infrared spectroscopy was performed to identify the functional groups present in the *Lactiplantibacillus plantarum* culture grown in Luria–Bertani (LB) broth. The recorded FTIR spectrum (Fig.3) exhibited distinct peaks at 604, 1021, 1408, 1638, 2095, and 3611 cm^{-1}, corresponding to the characteristic molecular vibrations of biomolecules secreted or present on the bacterial cell surface.

The absorption band observed at 604 cm^{-1} can be attributed to C–H deformation, indicating the possible presence of biomineral or organic residue interaction in the medium. The prominent peak at 1021 cm^{-1} is associated with C–O–C stretching or C–N stretching vibrations of polysaccharides and proteins, reflecting the metabolic activity of *Lactiplantibacillus plantarum*. The peak at 1408 cm^{-1} corresponds to the symmetric stretching of carboxylate ($–COO^-$) groups, which are typically derived from amino acids and fatty acids in the bacterial cell wall or extracellular secretions.

The strong peak observed at 1638 cm^{-1} represents the amide I band, primarily due to C=O stretching of peptide linkages in proteins, confirming the presence of proteinaceous biomolecules. A moderate peak at 2095 cm^{-1} may correspond to C≡C or C≡N stretching vibrations, indicating the presence of nitrile or alkyne groups, possibly arising from enzymatic or metabolic by-products. Finally, a broad peak at 3611 cm^{-1} is attributed to O–H stretching vibrations, indicating the presence of hydroxyl groups from water, alcohols, or phenolic compounds. The FTIR spectral profile confirms the presence of major biomolecular components such as proteins, carbohydrates, and lipids, which play a crucial role in the biosynthesis and stabilization of nanoparticles in subsequent biogenic synthesis experiments (Mukherjee *et al.* 2022). These functional groups serve as natural reducing and capping agents, making *Lactiplantibacillus plantarum* a potential *Candida*te for eco-friendly nanomaterial synthesis.

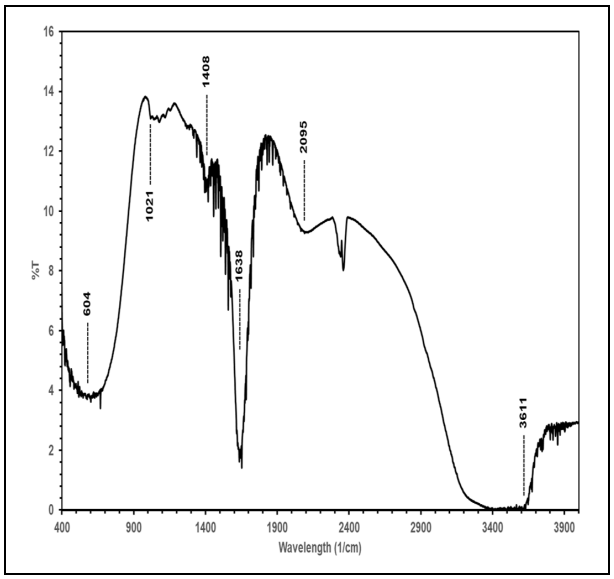


Fig. 3: FTIR spectrum of *Lactiplantibacillus plantarum sp.* grown in LB broth

3.3 FTIR Analysis of Synthesized SiO_2 NPs

The Fourier Transform Infrared spectra of *Lactiplantibacillus plantarum*-mediated and chemically synthesized SiO_2 NPs were recorded in the range of 4000–400 cm^{-1} to identify the surface functional groups and confirm nanoparticle formation (Fig.4). The Lb- SiO_2 NPs displayed prominent peaks at 466, 800, 956, 1044, 1099, 1463, 1634, 1745, and 3418 cm^{-1}. The strong peak around 466 cm-1 corresponds to Si–O–Si bending vibrations, confirming the formation of silicon oxide. The peaks at 800–1099 cm^{-1} represent asymmetric stretching vibrations of Si–O–Si and Si–O–H bonds, which are characteristic of silica structures. The peak at 1463–1634 cm^{-1} is attributed to amide I and II vibrations arising from C=O and N–H stretching of protein molecules secreted by *Lactiplantibacillus plantarum* sp., indicating their role as reducing and stabilizing agents during nanoparticle biosynthesis. The weak peak observed at 1745 cm^{-1} corresponds to C=O stretching of ester or carboxylic groups, while the broad band around 3418 cm^{-1} represents O–H stretching vibrations, confirming the presence of hydroxyl groups associated with adsorbed water and biomolecules on the nanoparticle surface.

The Ch– SiO_2 nanoparticles showed peaks at 652, 956, 1044, 1403, 1641, and 3618 cm^{-1}. The strong peak near 652 cm^{-1} corresponds to Si–O–Si bending, whereas the peaks between 956–1044 cm^{-1} confirm Si–O stretching vibrations, typical for silica frameworks. The peaks at 1403 and 1641 cm^{-1} correspond to C–O and C=O stretching vibrations, indicating the presence of residual organic or solvent molecules from the chemical synthesis process. The broad peak at 3618 cm^{-1} indicates the presence of surface hydroxyl groups, suggesting partial hydration or silanol formation.

The comparative analysis reveals that both synthesis routes successfully produced SiO_2 NPs, as evidenced by the characteristic Si–O–Si and Si–O–H vibrations. However, the *Lactiplantibacillus plantarum*-mediated SiO_2 NPs exhibit additional peaks related to protein and polysaccharide functional groups, confirming the biological capping and stabilization effect (Jamkhande *et al.* 2019; Kumar *et al.* 2021; Mahmud and Jahangir Hossain, 2024). These biomolecular interactions enhance nanoparticle stability and dispersion, making the biogenic route a more environmentally benign and effective approach for SiO_2 NPs synthesis.

3.4 XRD Analysis of SiO_2 NPs

The crystalline nature and phase composition of the *Lactiplantibacillus plantarum*–mediated and chemically synthesized SiO_2 NPs were examined using X-ray diffraction. Fig. 5 shows the diffraction pattern of the LP- SiO_2 NPs. The characteristic diffraction peaks at 2θ values corresponding to the (100), (101), (110), (111), (200), (102), (211), (202), (300), (310), (400), (333), (440), (620), and (622) planes match well with the standard SiO_2 NPs reference (JCPDS No. 27-0605).It exhibited a broad hump centered at 2θ ≈ 21.8°, characteristic of amorphous silica, as reported in the standard JCPDS Card No. 29-0085for SiO_2. Amorphous silicon dioxide does not display sharp, well-defined Bragg reflections, and therefore the broad peak rather than indexed crystalline planes confirm the formation of nanoscale amorphous silica. Minor low-intensity features were observed between 2θ = 26–35°, which may be attributed to surface silanol groups or short-range structural ordering within the amorphous network (Pednekar *et al.* 2017; Vazquez *et al.* 2017). The broadness of the peak suggests a small particle size and extensive surface disorder, consistent with biomolecule-mediated nucleation and growth in the *L. Plantarum* synthesis pathway.

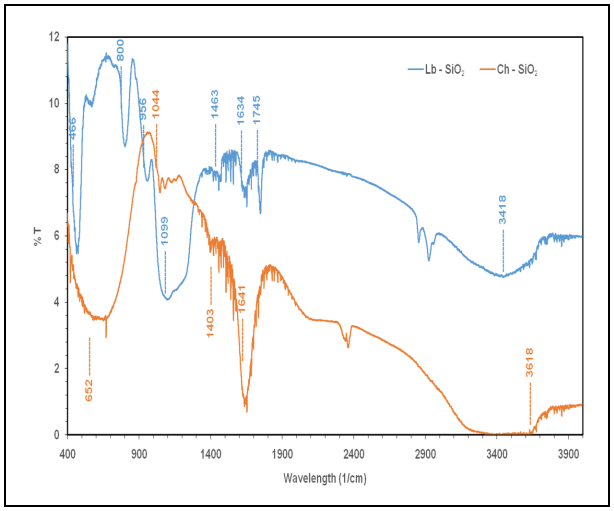


Fig. 4: FTIR spectra of Lb– SiO_2 and Ch– SiO_2 nanoparticles

Table 1. Comparative FTIR spectral peak assignment for Lb– SiO_2 and Ch– SiO_2 nanoparticles

Functional Group / Bond	*Lactiplantibacillus plantarum*	Lb– SiO_2 NPs	Ch– SiO_2 NPs
Si–O–Si	604	466, 800, 1044, 1099	652, 1044
C–O–C / C–N	1021	1044	1403
–COO^-	1408	1463	1403
C=O (Amide I)	1638	1634	1641
C≡C / C≡N	2095	-	-
O–H	3611	3418	3618
Si–O–H	-	956, 1099	956
C=O	-	1745	1641
N–H	-	3418	-
C–H	604	1463	-

The chemically synthesized SiO_2 NPs (Fig. 6) exhibited diffraction peaks at 2θ values corresponding to the (101), (100), (111), (200), (211), (220), (311), (400), (440), (422), and (511) planes are in good agreement with the standard SiO_2 pattern (JCPDS No. 27-0605), confirming the crystalline and phase-pure nature of the nanoparticles. The NPs also showed the characteristic amorphous silica halo at $2\theta \approx 22°$, matching JCPDS 29-0085, confirming the absence of crystalline impurities. Compared with the biogenic sample, the chemical synthesis produced a slightly sharper and more defined halo, indicating higher structural uniformity and reduced surface defect density, likely due to controlled reaction conditions. No additional crystalline peaks were detected in either sample, confirming high phase purity and the successful synthesis of amorphous SiO_2 NPs through both green and chemical routes.

The comparison highlights that both synthesis routes successfully produce phase-pure SiO_2 NPs, but with distinct structural characteristics. The *Lactiplantibacillus plantarum*-mediated synthesis leads to nanocrystalline SiO_2 with smaller crystallite size and moderate crystallinity, influenced by biomolecules that act as natural capping and stabilizing agents (Mahmud and Jahangir Hossain, 2024; Albalawi *et al.* 2022). Conversely, the chemical synthesis yields highly crystalline SiO_2 NPs with well-defined peaks and a more ordered lattice, owing to the absence of biological interference and the controlled growth environment (Ao *et al.* 2024). These structural variations are expected to influence the surface activity, optical properties, and potential applications of the nanoparticles in catalysis, sensing, and biomedical fields.

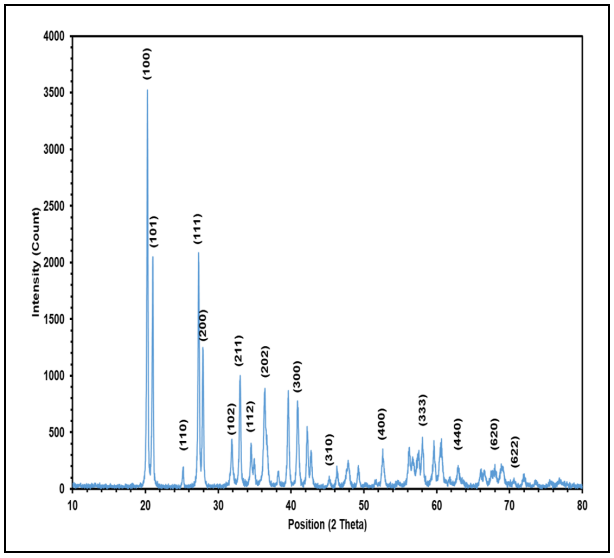


Fig. 5: XRD pattern of Lb - SiO_2 NPs

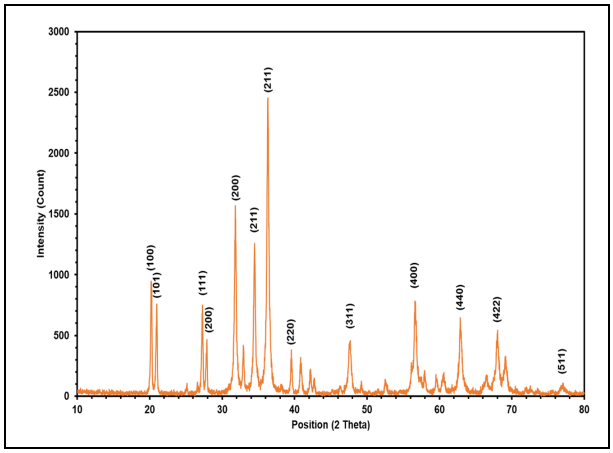


Fig. 6: XRD pattern of Ch - SiO_2 NPs

3.5 EDAX APEX Analysis of Synthesized SiO NPs

Evaluation of the EDX spectra for Lb– SiO_2 NPs and Ch– SiO_2 NPs revealed clear differences in elemental composition and surface purity, reflecting the influence of their respective synthesis methods.

The Lb– SiO_2 NPs showed strong and distinct peaks for silicon (Si) and oxygen (O), with no additional elemental signals detected (Fig. 7). The presence of only Si and O indicates a high level of elemental purity. Quantitative EDX values (Si: 58 wt%, 56 at%; O: 42 wt%, 44 at %) are consistent with silica-rich materials. Elemental mapping further demonstrated a uniform distribution of Si (63%) and O (37%) across the nanoparticle surface, suggesting efficient microbial-mediated stabilization. These results indicate that metabolites secreted by *L. Plantarum* contribute to a clean, carbon-free surface, characteristic of a biologically facilitated synthesis pathway.

In contrast, the Ch– SiO_2 NPs displayed three major peaks corresponding to Si, O, and C in the EDX spectrum (Fig. 8). The carbon signal is likely derived from residual organic precursors, surfactants, or solvent molecules retained from the chemical synthesis steps. Quantitative analysis showed Si (64 wt%, 36 at%), O (51 wt%, 49 at%), and C (43 wt%, 57 at%), and mapping revealed a uniform but noticeable distribution of carbon (16%). Although Si and O remain the dominant constituents, the presence of carbon suggests partial adsorption of synthesis by-products despite repeated washing.

Overall, EDX analysis confirms that both synthesis approaches successfully produce SiO_2 – containing nanoparticles, but differ substantially in elemental purity. The Lb – SiO_2 NPs exhibit a cleaner, carbon-free surface attributed to the biogenic synthesis route, whereas the chemically synthesized nanoparticles show residual carbon, reflecting the influence of chemical precursors. These differences highlight how synthesis methodology directly affects nanoparticle surface chemistry and potential application suitability.

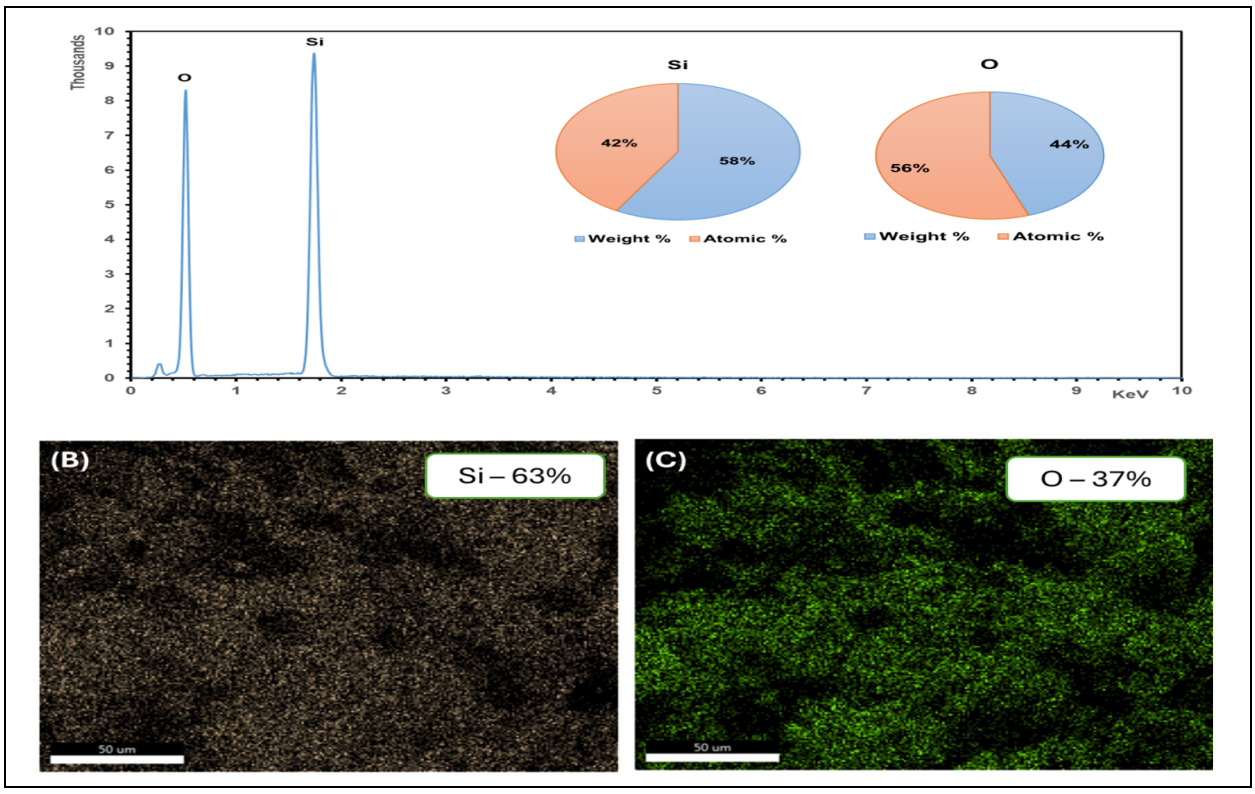


Fig. 7: Energy-Dispersive X-ray spectrum and elemental mapping of Lb– SiO_2 NPs. (A) EDAX spectrum showing major peaks for silicon (Si) and oxygen (O) confirming the formation of SiO_2; inset pie charts represent the weight and atomic percentage of Si and O. (B–C) Elemental mapping images showing uniform distribution of Si and O across the nanoparticle surface

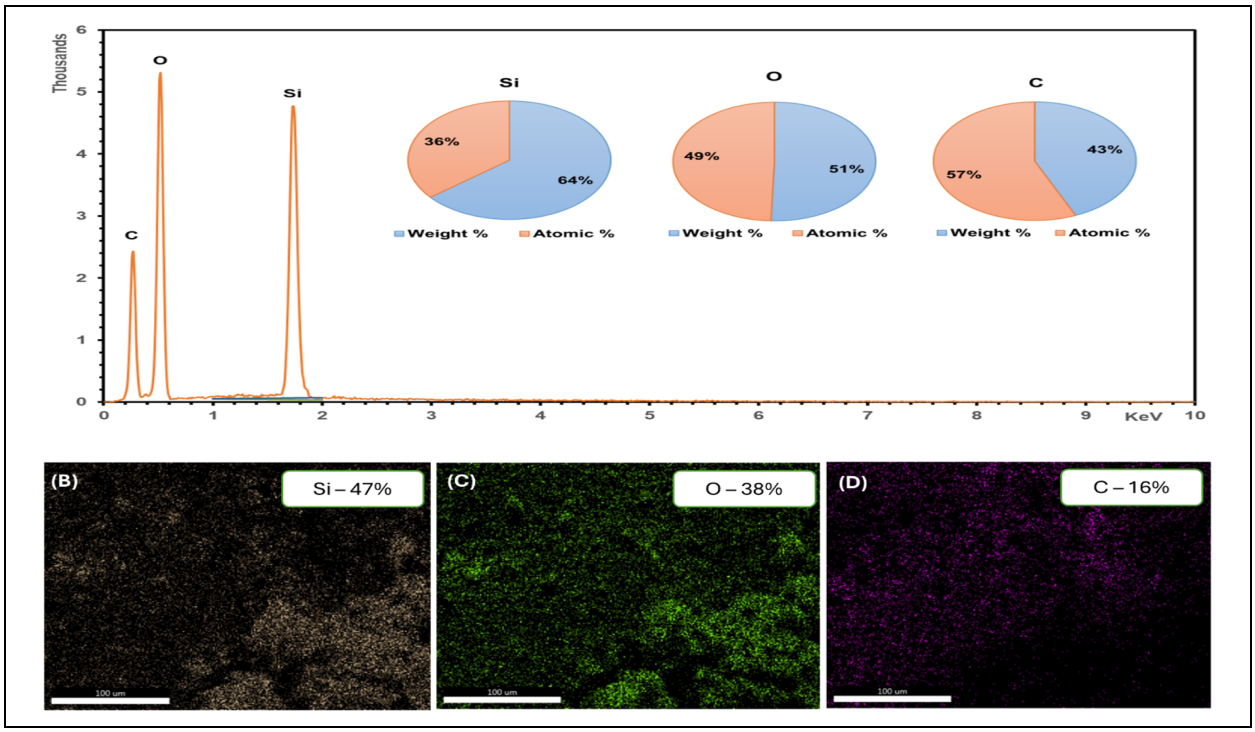


Fig. 8: Energy-Dispersive X-ray spectrum and elemental mapping of Ch– SiO_2 NPs. (A) EDAX spectrum showing major peaks for silicon (Si) and oxygen (O) confirming the formation of SiO_2; inset pie charts represent the weight and atomic percentage of Si and O. (B–C) Elemental mapping images showing uniform distribution of Si and O across the nanoparticle surface

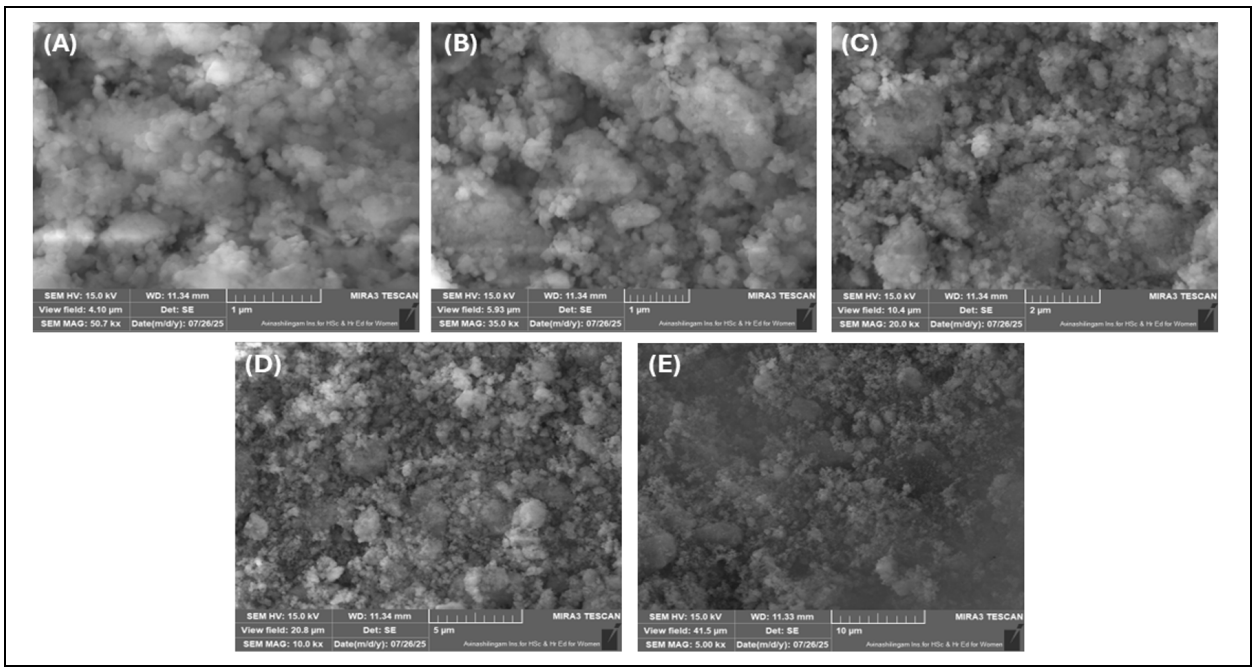


Fig. 9: FESEM micrographs of Lb– SiO_2 NPs at different magnifications (A–E)

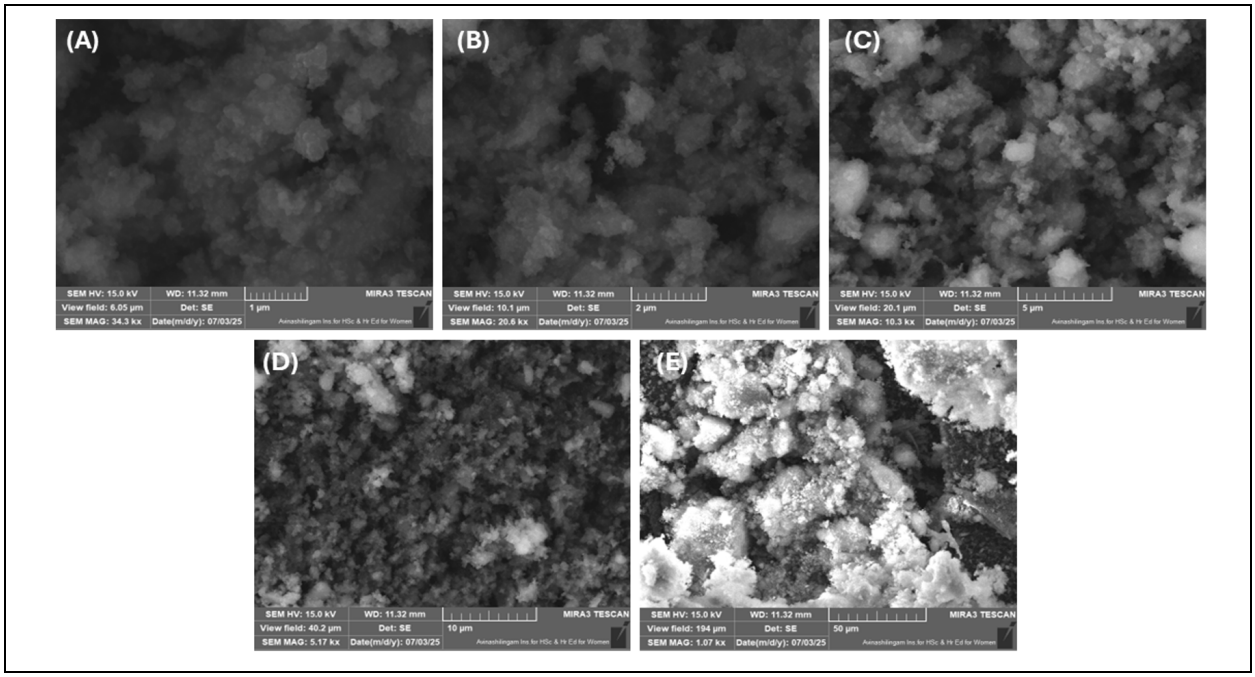


Fig. 10: FESEM micrographs of Ch– SiO_2 NPs at varying magnifications (A–E)

3.6 FESEM Analysis of Lb– SiO_2 and Ch– SiO_2 Nanoparticles

The surface morphology and structural features of both Lb– SiO_2 NPs and Ch– SiO_2 NPs were investigated using FESEM are presented in Fig.9 and 10, respectively. Distinct differences in particle morphology, size, and surface texture were observed between the two synthesis routes, indicating the influence of biological and chemical parameters on nanoparticle formation.

The FESEM micrographs of Lb– SiO_2 NPs revealed irregularly shaped, nearly spherical nanoparticles that were moderately aggregated into porous clusters. The aggregation pattern observed in the biogenic nanoparticles can be attributed to the presence of biomolecular capping agents such as proteins, enzymes, and polysaccharides secreted by *Lactiplantibacillus plantarum* during biosynthesis. These organic components facilitate particle stabilization and prevent uncontrolled growth but simultaneously induce

surface roughness and mild agglomeration (Albalawi *et al.* 2022; Mahmud and Jahangir Hossain, 2024). The porous and network-like structure also suggests high surface area, which is beneficial for catalytic and adsorption-based applications.

The chemically synthesized SiO_2 NPs exhibited a more uniform spherical morphology with smaller and well-dispersed particles. The Ch– SiO_2 NPs displayed smoother surfaces and compact packing, reflecting enhanced control over nucleation and growth under chemical synthesis conditions (Jamkhande *et al.* 2019). The absence of organic biomolecules resulted in reduced surface roughness and lower aggregation, contributing to a denser and more homogeneous microstructure. The bright contrast regions visible in low-magnification images further indicate higher crystallinity, consistent with the XRD findings.

3.7 Dynamic Light Scattering Analysis of Synthesized Nanoparticles

The particle size distribution of the synthesized silicon oxide nanoparticles (SiO_2 NPs) was determined using Dynamic Light Scattering (DLS), and the results are illustrated in Fig.11. As shown in Fig.11(A), Lb– SiO_2 NPs exhibited a narrow and monomodal distribution, with an average particle size around 194 ± 19.44 nm. The sharp intensity peak indicates that the biosynthesized nanoparticles are relatively uniform in size, suggesting effective nucleation during the biomineralization process. The slightly larger hydrodynamic diameter compared to the primary particle size observed in FESEM is attributed to the presence of capping biomolecules and the hydration layer surrounding the nanoparticles in suspension (Kumar *et al.* 2021). The biological synthesis process, mediated by *Lactiplantibacillus plantarum* secretions, likely contributes to improved colloidal stability and reduced agglomeration due to natural surface functionalization.

The Ch– SiO_2 NPs displayed a broader particle size distribution with an average size of approximately 332 ± 24.37 nm, as shown in Fig.11(B). The wider size range and slight shift toward higher diameters indicate the occurrence of mild aggregation in the chemically produced nanoparticles, possibly due to the absence of natural stabilizing agents (Nyabadza *et al.* 2023; Jamkhande *et al.* 2019). Nevertheless, the relatively narrow distribution pattern demonstrates good control over particle formation, consistent with the uniform morphology observed in FESEM micrographs. Comparatively, the Lb– SiO_2 NPs show smaller and more monodisperse particle sizes, attributed to the biomolecular capping and controlled nucleation offered by the biological synthesis route. Meanwhile, the Ch– SiO_2 NPs exhibit larger, more aggregated particles due to the physicochemical reaction dynamics inherent to chemical synthesis.

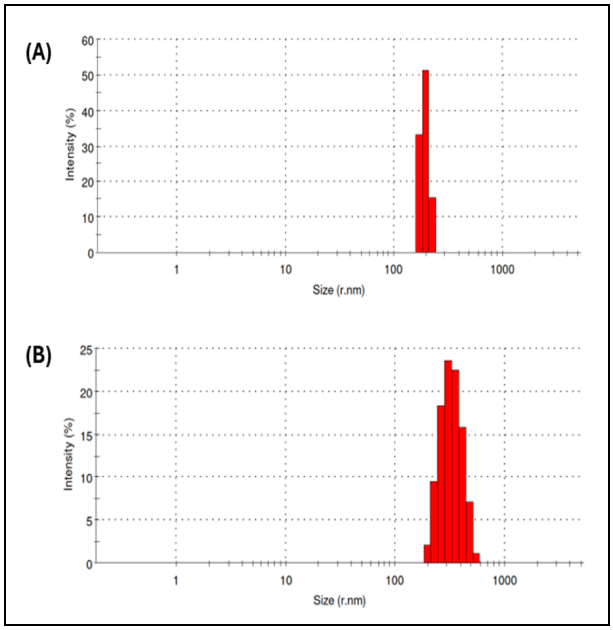


Fig. 11: Particle size distribution of (A) Lb– SiO_2 NPs and (B) Ch– SiO_2 NPs obtained from DLS analysis

3.8 Zeta Potential Analysis of Lb– SiO_2 and Ch– SiO_2 Nanoparticles

The surface charge and colloidal behavior of the synthesized SiO_2 NPs were evaluated using zeta potential measurements, as shown in Fig. 12.The Lb– SiO_2 NPs exhibited a zeta potential of –0.30 mV (Fig. 12A). Such a low zeta potential indicates that the particles possess very weak electrostatic repulsion and are not electrostatically stable in suspension. The near-neutral charge likely arises from surface silanol (Si–OH) groups partially neutralized by biomolecules, such as proteins and polysaccharides, derived from *L. Plantarum* during biosynthesis (Gregirchak *et al.* 2023; Kumar *et al.* 2021). Although the electrostatic stability is poor, these biomolecular coatings may contribute some degree of steric stabilization, which can delay, but not fully prevent, aggregation. The narrow peak in the distribution profile reflects uniformity in the surface chemistry, consistent with the DLS results.

The Ch– SiO_2 NPs showed a zeta potential of +14.5 mV (Fig. 12B). This value is also below the accepted threshold for stable colloids, indicating limited electrostatic stabilization and a greater likelihood of aggregation, which aligns with the broader particle size distribution observed in DLS (Pal *et al.* 2018; Nyabadza *et al.* 2023). The low surface charge may arise from insufficient ionization of surface silanol groups and the absence of organic stabilizers. Overall, neither Lb– SiO_2 NPs nor Ch– SiO_2 NPs exhibit strong electrostatic stability, as their zeta potential values fall below the commonly accepted stability criterion (≥ 30 mV). However, the biomolecular capping present on Lb– SiO_2 NPs may provide supplementary steric effects that

improve dispersion relative to chemically synthesized particles. These findings highlight that the colloidal behavior of biogenic SiO_2 NPs is influenced more by surface-bound organic molecules than by electrostatic charge alone.

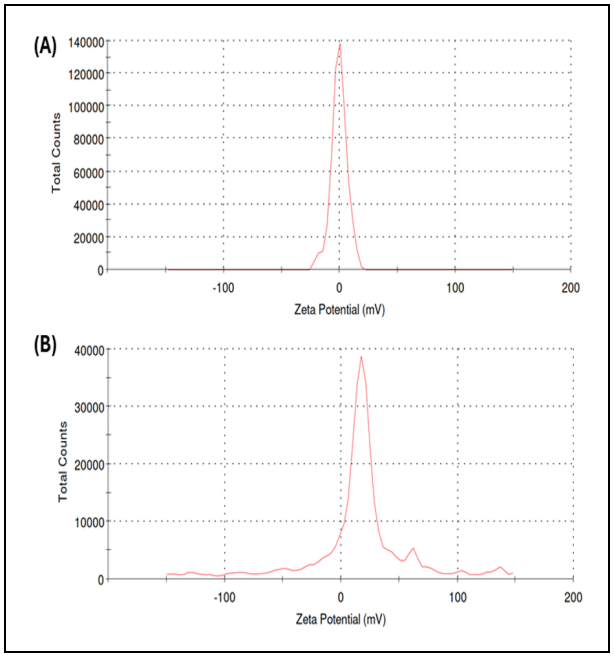


Fig. 12: Zeta potential distribution curves of (A) Lb– SiO_2 NPs and (B) Ch– SiO_2 NPs

3.9 Antioxidant Activity (DPPH Radical Scavenging Assay)

The antioxidant potential of the synthesized SiO_2 NPs was evaluated using the DPPH free radical scavenging assay, as represented in Fig.13. The scavenging efficiency of Lb– SiO_2 NPs, Ch– SiO_2 NPs, and the standard antioxidant L-ascorbic acid was analysed across a concentration range of 20 to 120 µg/mL. A clear dose-dependent increase in radical scavenging activity was observed for all the tested samples. Among them, L-ascorbic acid exhibited the highest DPPH inhibition, reaching approximately 83.7% at a concentration of 120 µg/mL, serving as a positive control for comparison.

The Lb– SiO_2 NPs demonstrated a higher antioxidant activity, with nearly 75.4% inhibition at 120 µg/mL, compared to Ch– SiO_2 NPs, which exhibited around 68.2% inhibition at the same concentration. The calculated IC50 values, representing the concentration required to inhibit 50% of the DPPH radicals, were found to be 45.6 µg/mL for L-ascorbic acid, 58.3 µg/mL for Lb–SiO_2 NPs, and 67.9 µg/mL for Ch– SiO_2 NPs. The lower IC_{50} value of Lb– SiO_2 NPs compared to Ch– SiO_2 NPs indicates a higher free radical scavenging efficiency, suggesting that the biologically synthesized nanoparticles possess enhanced antioxidant properties (Albalawi *et al.* 2022; Mahmud and Jahangir Hossain, 2024).

This improvement in antioxidant capacity can be attributed to the presence of bioactive capping molecules derived from *Lactiplantibacillus plantarum* metabolites such as proteins, phenolic compounds, and polysaccharides. These biomolecules introduce functional groups like hydroxyl (–OH), amino ($–NH_2$), and carboxyl (–COOH) that can donate protons or electrons to neutralize DPPH radicals, thereby enhancing the scavenging activity of the nanoparticles. The linear regression equations obtained for each sample were Inh = 0.456x + 17.04 (R2 = 0.897) for Lb– SiO_2 NPs, Inh = 0.510x + 9.318 (R2 = 0.882) for Ch– SiO_2 NPs, and Inh = 0.509x + 23.76 (R2 = 0.981) for L-ascorbic acid. The high correlation coefficients (R2> 0.88) confirm a strong linear relationship between nanoparticle concentration and scavenging efficiency (Mukherjee *et al.* 2022; Jamkhande *et al.* 2019). The results suggest that Lb– SiO_2 NPs exhibit superior antioxidant activity compared to Ch– SiO_2 NPs, confirming that biological synthesis using *Lactiplantibacillus plantarum* enhances the functional and reactive surface characteristics of SiO_2 NPs, leading to improved free radical scavenging performance.

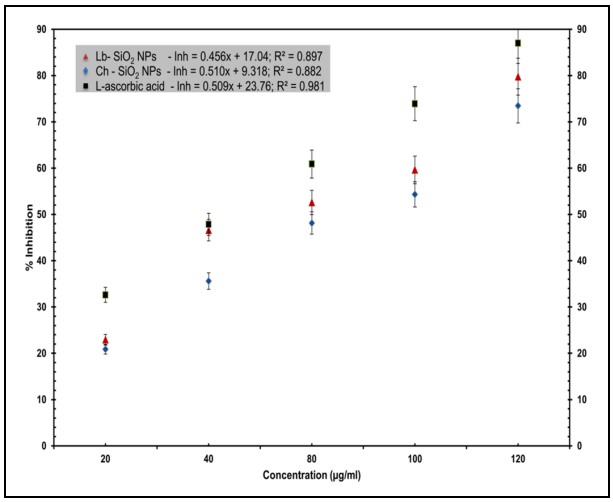


Fig. 13: DPPH radical scavenging activity of Lb– SiO_2, Ch–SiO_2, and L-ascorbic acid at various concentrations (20–120 µg/mL)

3.10 Antifungal Activity of Synthesized Nanoparticles Against Fluconazole-resistant *Candida parapsilosis*

The antifungal activity of the synthesized SiO_2 NPs was assessed against fluconazole- resistant *Candida parapsilosis* using the agar well diffusion method, and the results are presented in Fig.14& 15. Both Lb– SiO_2 NPs and Ch– SiO_2 NPs exhibited concentration-dependent inhibitory effects, with the zone of inhibition (ZOI) increasing up to an optimal concentration and decreasing at higher concentrations, possibly due to

nanoparticle aggregation and reduced bioavailability (Martins *et al.* 2023; Li *et al.* 2020).

At 100 µg/mL, the Lb– SiO_2 NPs exhibited the highest antifungal activity with a ZOI of 27.1 ± 1.4 mm, while the Ch– SiO_2 NPs showed a slightly lower inhibition zone of 24.6 ± 1.2 mm. In comparison, the control demonstrated a ZOI of 21.0 ± 0.9 mm under the same experimental conditions. The regression analysis for Lb– SiO_2 NPs showed a correlation coefficient of R2 = 0.849 (y = −0.544x2 + 3.355x + 17.35), while Ch– SiO_2 NPs displayed R2 = 0.708 (y = −0.696x2 + 3.946x + 18), indicating a strong polynomial relationship between nanoparticle concentration and antifungal efficiency (Masood *et al.* 2022).

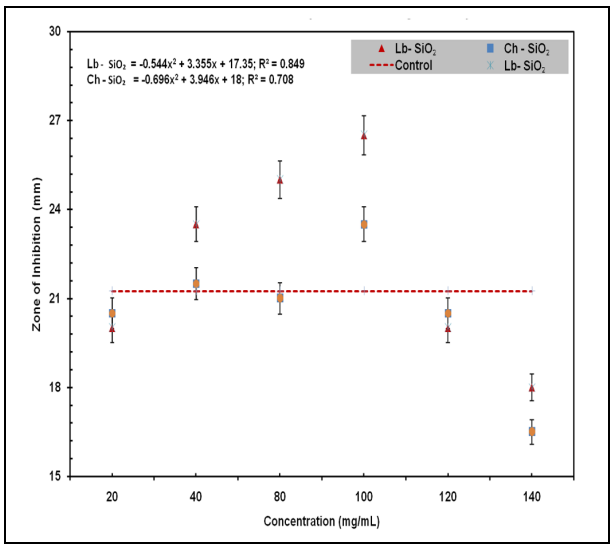


Fig. 14: Antifungal activity of Lb– SiO_2 and Ch– SiO_2 NPs against fluconazole-resistant *Candida parapsilosis*

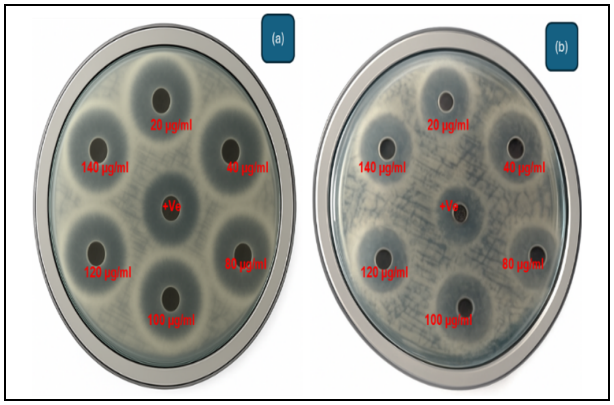


Fig. 15: Agar well diffusion assay demonstrating the antifungal activity of silicon oxide nanoparticles against *Candida parapsilosis* (a) Lb– SiO_2 NPs, (b) Ch– SiO_2 NPs

The superior antifungal activity of the Lb– SiO_2 NPs compared to the chemically synthesized ones can be attributed to the presence of bioactive surface molecules derived from *Lactiplantibacillus plantarum* metabolites, which may enhance cell membrane interaction and disrupt the fungal cell wall integrity more effectively (Ao *et al.* 2024). These biofunctionalized nanoparticles likely induce oxidative stress and inhibit ergosterol synthesis, leading to cell membrane destabilization and cell death in *C. parapsilosis*. The Ch– SiO_2 NPs, lacking such biological surface coatings, exhibited comparatively lower activity, though still significant inhibition was observed relative to the control (21 ± 0.9 mm). This suggests that both types of SiO_2 NPs possess antifungal potential, but the biomediated route enhances their functional efficacy and biocompatibility.

4. CONCLUSION

The present study successfully synthesized silicon oxide nanoparticles using both *Lactiplantibacillus plantarum*-mediated and chemically synthesized approaches and comprehensively characterized their physicochemical and biological properties. Comparative analysis confirmed that the green, *Lactiplantibacillus plantarum*-assisted route produced nanoparticles with superior structural and functional attributes. The UV–Visible spectra revealed distinct absorption peaks at 225 nm and 220 nm for Lb– SiO_2 and Ch– SiO_2 NPs, respectively, confirming nanoscale formation, with the stronger absorbance of Lb– SiO_2 NPs indicating enhanced dispersion and reduced agglomeration due to biological capping. FTIR spectroscopy confirmed characteristic Si–O–Si and Si–O–H vibrations in both samples, while additional amide and hydroxyl peaks in Lb– SiO_2 NPs confirmed the presence of protein and polysaccharide biomolecules acting as natural reducing and stabilizing agents. XRD analysis confirmed crystalline SiO_2 NPs formation with patterns consistent with JCPDS No. 29-0085, showing sharper peaks and higher crystallinity for Ch– SiO_2 NPs, whereas Lb– SiO_2 NPs exhibited mixed amorphous-crystalline features due to biomolecular interactions. FESEM images revealed that Lb– SiO_2 NPs were predominantly spherical, and less aggregated, while Ch– SiO_2 NPs displayed irregular morphology and partial clustering. EDX analysis confirmed high elemental purity of Si and O in both cases. Zeta potential measurements indicated greater colloidal stability for Lb– SiO_2 NPs (–0.3 mV) compared to Ch– SiO_2 NPs (14.5 mV), attributed to the presence of negatively charged biomolecular coatings. Particle size analysis supported nanoscale formation with smaller mean diameters for the biogenic nanoparticles. Biologically, Lb– SiO_2 NPs exhibited superior antioxidant activity (IC50 = 58.3µg/mL) and higher antifungal efficacy against Fluconazole-resistant *Candida parapsilosis* (27.1 ± 1.4 mm at 100 mg/mL) compared to Ch– SiO_2 NPs (24.6 ± 1.2 mm).These findings establish that *Lactiplantibacillus plantarum*-mediated synthesis offers an eco-friendly, sustainable, and effective alternative to chemical routes, yielding highly stable, monodispersed, and bioactive SiO_2 NPs

suitable for biomedical, pharmaceutical, and antimicrobial applications.

ACKNOWLEDGEMENT

We acknowledge the management of Sri Krishna Arts and Science College, Coimbatore, Tamil Nadu, India for providing necessary facilities to carry out this study.

We acknowledge the DST-FIST supported Central Instrumentation Laboratory facility of RVS College of Arts and Science, Coimbatore, for extended laboratory support to accomplish the analysis of nanoparticles.

FUNDING

This research received no specific grant from any funding agency in the public, commercial, or not-for-profit sectors.

CONFLICTS OF INTEREST

The authors declare that there is no conflict of interest.

COPYRIGHT

This article is an open-access article distributed under the terms and conditions of the Creative Commons Attribution (CC BY) license (http://creativecommons.org/licenses/by/4.0/).



REFERENCES

Albalawi, M. A., Abdelaziz, A. M., Attia, M. S., Saied, E., Elganzory, H. H. and Hashem, A. H., Mycosynthesis of Silica Nanoparticles Using *Aspergillus niger*: Control of *Alternaria solani* Causing Early Blight Disease, Induction of Innate Immunity and Reducing of Oxidative Stress in Eggplant, *Antioxid.,* 11(12), 2323 (2022). https://doi.org/10.3390/antiox11122323

Alcoceba, E., Gómez, A., Lara-Esbrí, P., Oliver, A., Beltrán, A. F., Ayestarán, I., Muñoz, P., Escribano, P. and Guinea, J., Fluconazole-resistant *Candida parapsilosis* Clonally Related Genotypes: First Report Proving the Presence of Endemic Isolates Harbouring the Y132F ERG11 Gene Substitution in Spain, *Clin. Microbiol. Infect*., 28(8), 1113–1119 (2022). https://doi.org/10.1016/j.cmi.2022.02.025

Ao, L. H., Wei, Y. G., Tian, H. R., Zhao, H., Li, J. and Ban, J. Q., Advances in the Study of Silica Nanoparticles in Lung Diseases, *Sci. Total Environ.,* 912, 169352 (2024). https://doi.org/10.1016/j.scitotenv.2023.169352

Cavalheiro, M. and Teixeira, M. C., *Candida* Biofilms: Threats, Challenges, and Promising Strategies, *Front. Med.*, 5, 28 (2018). https://doi.org/10.3389/fmed.2018.00028

Ding, R., Li, Y., Yu, Y., Sun, Z. and Duan, J., Prospects and Hazards of Silica Nanoparticles: Biological Impacts and Implicated Mechanisms, *Biotechnol. Adv.*, 69, 108277 (2023). https://doi.org/https://doi.org/10.1016/j.biotechadv.2023.108277

Gregirchak, N., Syniavska, D., Khonkiv, M. and Stabnikov, V., Lactic Acid Bacteria for the Synthesis of Metals Nanoparticles, *Biotechnol. Microbiol. Ukr. Food J.*, 12(4), 599-626(2023). https://doi.org/10.24263/2304- 974X-2023-12-4- 8

Jamkhande, P. G., Ghule, N. W., Bamer, A. H. and Kalaskar, M. G., Metal Nanoparticles Synthesis: An Overview on Methods of Preparation, Advantages and Disadvantages, and Applications, *J. Drug Deliv. Sci. Technol.*, 53, 101174 (2019). https://doi.org/10.1016/j.jddst.2019.101174

Kumar, J. A., Krithiga, T., Manigandan, S., Sathish, S., Renita, A. A., Prakash, P., Prasad, B. S. N., Kumar, T. R. P., Rajasimman, M., Hosseini-Bandegharaei, A., Prabu, D. and Crispin, S., A Focus to Green Synthesis of Metal/Metal-Based Oxide Nanoparticles: Various Mechanisms and Applications Towards Ecological Approach, *J. Clean. Prod*., 324, 129198 (2021). https://doi.org/10.1016/j.jclepro.2021.129198

Li, J., Ding, Z., Li, Y., Miao, J., Wang, W., Nundlall, K. and Chen, S., Reactive Oxygen Species-Sensitive Thioketal-Linked Mesoporous Silica Nanoparticles as Drug Carrier for Effective Antibacterial Activity, *Mater. Des.,* 195, 109021 (2020). https://doi.org/10.1016/j.matdes.2020.109021

Mahmud, M. and Jahangir Hossain, M., A Review on Eco-Friendly Silica Nanoparticles and Their Applications, *J. Med. Nanomater. Chem*., 6(3), 208–225 (2024). https://doi.org/10.48309/JMNC.2024.3.4

Martins S. F. P., Higor, R. M. P., Lopes, A. A., Barros, A. C. L. J., Azevedo, P. A., Itala, G. A. M., Carneiro, M. S., Alves, V. M., Gonçalvez, C. F. S., Barbosa, G. T., Gonzaga, F. L. L., Henrique, S. S. E., Holanda, T. E. and Longhinotti, E., Antibacterial and Antifungal Action of CTAB-Containing Silica Nanoparticles Against Human Pathogens, *Int. J. Pharm.,* 641, 123074 (2023). https://doi.org/10.1016/j.ijpharm.2023.123074

Masood, S. A., Maheen, S., Khan, H. U., Zafar, M. N., Shafqat, S. S., Mujtaba, M. A., ur Rehman, A., Abbas, G., Mahmood, M. H. R., Bashir, S., Yunus Khan, T. M. and Khalifa, A. S., In Vitro/In Vivo Evaluation of Statistically Engineered Alginate Scaffold Reinforced with Dual Drugs Loaded Silica Nanoparticles for Enhanced Fungal Therapeutics, *Alex. Eng. J.,* 61(5), 4041–4056 (2022). https://doi.org/10.1016/j.aej.2021.09.027

Maťátková, O., Michailidu, J., Miškovská, A., Kolouchová, I., Masák, J. and Čejková, A., Antimicrobial Properties and Applications of Metal Nanoparticles Biosynthesized by Green Methods, *Biotechnol. Adv.,* 58, 107905 (2022). https://doi.org/10.1016/j.biotechadv.2022.107905

Mukherjee, N., Sil, M., Adak, S., Mukherjee, A. and Goswami, A., The Biosafety Study of SiO_2 Nanoparticle on Lactic Acid Bacillus—An Approach Towards Safety on Human Gut Immunity, *J. Med. Pharm. Allied Sci.*, 11(3), 4939–4946 (2022). https://doi.org/10.55522/jmpas.V11I3.3763

Nazaralian, S., Majd, A., Irian, S., Najafi, F., Ghahremaninejad, F., Landberg, T. and Greger, M., Comparison of Silicon Nanoparticles and Silicate Treatments in Fenugreek*, Plant Physiol. Biochem.,* 115, 25–33 (2017). https://doi.org/10.1016/j.plaphy.2017.03.009

Pal, G., Rai, P. and Pandey, A., Green Synthesis of Nanoparticles: A Greener Approach for a Cleaner Future, *Green Synth. Charact. Appl. Nanopart.,* 1–26 (2018). https://doi.org/10.1016/B978-0-08-102579-6.00001-0

Pednekar, P. P., Godiyal, S. C., Jadhav, K. R. and Kadam, V. J., Mesoporous Silica Nanoparticles: A Promising Multifunctional Drug Delivery System, *Nanostructures Cancer Ther*., 593–621 (2017). https://doi.org/10.1016/B978-0-323-46144-3.00023-4

Vazquez, N. I., Gonzalez, Z., Ferrari, B. and Castro, Y., Synthesis of Mesoporous Silica Nanoparticles by Sol-Gel as Nanocontainer for Future Drug Delivery Applications, *Bol. Soc. Esp. Ceram. Vidrio*, 56(3), 139–145 (2017). https://doi.org/10.1016/j.bsecv.2017.03.002